Photodegradation of microcystin-LR by pyridyl iron porphyrin immobilized on NaY zeolite

Shulian Wang, Huiqin Zhang, Hongmei Ge, Yafei Shi and Zhu Li

ABSTRACT

A novel photocatalyst, FeTPyPY, was prepared by immobilizing water-soluble tetra(4-pyridyl)phenyl iron-porphyrin (FeTPyP) on NaY zeolite to degrade microcystin-LR (MC-LR), one of the most toxic microcystins (MCs). UV-Vis analysis, UV-Vis diffuse reflectance spectroscopy, infrared spectroscopy, cyclic voltammetry and transmission electron microscopy were employed to characterize immobilized FeTPyPY. Under visible light ($\lambda \geq 420$ nm), MC-LR was degraded utilizing immobilized FeTPyPY by activating molecular oxygen. The results showed that 85% of MC-LR was efficiently degraded by FeTPyPY with loading amount 100:1 (m_{NaY}:m_{FeTPyP}) after 300 min of visible light illumination. Moreover, FeTPyPY was stable in the degradation system with pH 7.0. The degradation mechanism was evaluated using electron spin resonance, and the results demonstrated that highly reactive oxygen species (•OH radical) were generated in the system to degrade MC-LR. Therefore, immobilized FeTPyPY was available to break down the toxic groups within MC-LR by utilizing environmental •OH radical under circumneutral condition.

Key words | immobilization, MC-LR, photocatalysis, tetra(4-pyridyl)phenyl iron-porphyrin

Shulian Wang (corresponding author)
Huiqin Zhang
Hongmei Ge
Yafei Shi
Zhu Li
Hubei Key Laboratory of Ecological Remediation for Rivers-Lakes and Algal Utilization, School of Civil Engineering, Architecture and Environment,
Hubei University of Technology,
Wuhan 430068,
China
E-mail: *wangshulian@hbut.edu.cn*

Shulian Wang
Advanced Environmental Biotechnology Centre,
Nanyang Environment & Water Research Institute,
Nanyang Technological University,
1 Cleantech Loop, Singapore 637141,
Singapore

INTRODUCTION

Microcystin-LR (MC-LR) (Figure S1, Supplementary Information), a hepatotoxin produced from cyanobacteria in eutrophic surface waters, is a serious threat to aquatic life and humans (Brunberg & Blomqvist 2002; Holst *et al.* 2003). It targets the liver and inhibits phosphatase 1 and 2A to strongly promote tumor (Yasmin *et al.* 2019). Because of the potent toxicity, the International Agency for Research on Cancer has classified MC-LR as possibly carcinogenic to humans (Group 2B) and the guideline value set by the World Health Organization for MC-LR in drinking water is 1 μg/L. MC-LR pollution in surface water has become a global environmental problem and attracts increasing attention (Mantzouki *et al.* 2018; Hu & Rzymski 2019; Henao *et al.* 2020). Conventional water treatments such as coagulation and activated carbon adsorption achieved limited success in removing MC-LR effectively (Han *et al.* 2013; Phujomjai *et al.* 2015). Advanced oxidation processes (AOPs) with the generation of hydroxyl radical (•OH) is considered to be the most promising method in the detoxification of MC-LR in contaminated water (Krzywicka & Kwarciak-Kozłowska 2014).

The hydroxyl radical is an active species with high oxidation potential ($E_0 = 2.76$ V); thus, its oxidation activity is strong and its effect on the transformation of harmful substances in the natural environment is important (Li *et al.* 2019). Therefore, significantly increased research has focused on the different ways in which •OH is produced, and on how to produce •OH faster and more efficiently. However, almost all of these systems about MC-LR degradation are dissolving MC-LR in pure water without considering the presence of natural organic matter (NOM). The •OH reacts more preferentially with high concentration of NOM than with trace quantities of MC-LR. Therefore, these methods are still difficult to be used in the presence of NOM. Generally, the concentration of MC-LR is lower than 10 ppm in algae-bloom water, while the concentration of NOM is normally in the range from 10 to 100 ppm (Aschermann *et al.* 2016). In real scenarios, MC-LR degradation by AOPs is inefficient, and consequently, environmentally friendly methods for MC-LR removal in the existence of NOM are significantly important.

In the studies about contaminant degradation in the presence of NOM, researchers found that variable-valent metal catalysts may be similar to specific enzymes with high selectivity, which could provide special catalytic sites for the degradation of pollutants in nature (Yanina & Rosso 2008; Schreiner *et al.* 2011; Katz *et al.* 2012). Since

doi: 10.2166/wst.2020.083

Meunier and coworkers succeeded in the degradation of 2,4,6-trichloropenol utilizing water-soluble iron tetrasulfophthalocyanine (FePcS) as the catalyst in mixed solvent with acetonitrile and H_2O (Sorokin *et al.* 1996), the complexes of metal and organics used as photocatalyst for the treatment of pollutants have received a lot of attention (Kim *et al.* 2005; Tang *et al.* 2019). Due to the variable valence state of metals or the interactions between metals and molecular oxygen or other ligands, soluble or immobilized metal porphyrins have been widely applied as selective oxidant of toxic pollutants (Peng *et al.* 2015; Rahimi *et al.* 2015; Günay & Cimen 2017; Gamelas *et al.* 2018). Song and coworkers discussed the physicochemical properties of homogeneous and heterogeneous high-valent Fe(IV)-O species and proved that Fe(IV)-O compounds had the characteristics of p450-like enzyme in the oxidation reaction (Song *et al.* 2005). Iron porphyrin is a promising catalyst to remove organic pollutants in our environment, and immobilization on inert carriers is an effective approach to enhance stability and selectivity (Wang *et al.* 2019).

In this work, a green processing system consisting of metalloporphyrins immobilized on an inert carrier in the presence of visible irradiation and O_2 was established. Immobilized photocatalyst, FeTPyPY, was prepared and its photocatalytic activity and the influence of operational parameters on the degradation of MC-LR was investigated.

MATERIALS AND METHODS

Materials

Tetra(4-pyridyl)phenyl porphyrin (TPyP) (Figure S2, Supplementary Information) was obtained from J&K Scientific Co. NaY zeolite was purchased from Tianjin Tianli Chemical Reagent Co. 5,5-Dimethyl-1-pyrroline-*N*-oxide (DMPO) and N,N-diethyl-*p*-phenylenediamine (DPD) were provided by Sigma-Aldrich Co. MC-LR (95%) was purchased from Express Technology Co. Technical grade humic acid (HA) was purchased from Sigma-Aldrich Co. Chromatographically pure grade methanol, acetonitrile and trifluoroacetic acid (TFA) were obtained from Merck Co. Ultrapure water was used throughout the experiment. The pH was adjusted with either NaOH (1 mol/L) or $HClO_4$ (1 mol/L).

Preparation of FeTPyP

FeTPyP was prepared according to a reported procedure (Li *et al.* 2012). A three-neck flask (25 mL) containing 10 mL of $Fe(NO_3)_3$ (2.5×10^{-3} mol/L) solution and 5 mg of TPyP was heated with continual stirring. At different intervals, 10 mL of reaction solution was extracted to measure the absorbance at 200–700 nm. Changes in absorbance and appearance of new absorption bands were observed. The reaction was stopped when changes in the Soret-band disappeared and new peaks appeared. After the reaction, excess Fe^{3+} was removed using IRA200 cation exchange resin.

Preparation of FeTPyPY

NaY zeolite and FeTPyP (*m*/*m* 10:1, 20:1, 100:1, 200:1) were stirred in a container for 24 h under ambient conditions. Immobilized FeTPyPY with different loadings were separated by filtration, rinsed with water until no FeTPyP was detected, and finally dried at 50 °C. The corresponding photocatalytic results (Figure S3) demonstrated that FeTPyPY with loading amount 100:1 had the maximum degradation rate. Therefore, all the other degradation experiments were carried out with it.

Catalyst characterization

A Lambda 25 UV-Vis spectrophotometer (Perkin Elmer, USA) was used to obtain UV-visible absorption spectra. UV-visible diffuse reflectance spectroscopy (UV-Vis DRS) was carried out using a U-3010 UV-Vis spectrophotometer (Hitachi, Japan) using spectral grade $BaSO_4$ as the reference material. Infrared (IR) analysis was carried out with a Nicolet Nexus FTIR spectrophotometer (Thermo Electron, USA). The cyclic voltammetry (CV) curves were obtained on a CHI660E electrochemical workstation (Chenhua, China). The morphology was characterized with transmission electron microscopy (TEM).

Photocatalytic procedures and analyses

The reaction was carried out in a Pyrex vessel containing 5 mL of MC-LR (2 mg/L) and 5 mg of FeTPyPY. The vessels were put into an XPA series instrument using a 500-W halogen lamp (Institute of Electric Light Source, Beijing, China) as the light source. To ensure visible illumination, a filter was placed in the middle of the vessel and lamp to eliminate any radiation at wavelength below 420 nm. Prior to illumination, a reaction suspension was continuously stirred in the dark for half an hour to ensure establishment of MC-LR adsorption/desorption equilibrium on the surface of FeTPyPY. After the reaction started, 300 μL of the reaction suspension was obtained at given irradiation time intervals, and then centrifuged (8,000 r/min) and filtered

through a Millipore filter (0.22 μm) to remove FeTPyPY particles.

A Waters 600 high performance liquid chromatograph (Waters, USA) equipped with a Waters 2998 photodiode array detector and C18 reverse phase column (5 μm, 4.6 mm i.d. × 250 mm, Kromasil) was employed to determine the concentration of MC-LR at the wavelength of 238 nm. The mobile phase was methanol and 0.05% TFA (*v*/*v*) (65:35). The injection volume of samples was 20 μL and the flow rate was 0.6 mL/min.

Liquid chromatography–mass spectrometry (LC/MS) (Agilent, USA) was employed to monitor the degradation intermediates with scanning range from *m*/*z* 300 to 1,200 in positive ion mode. Formic acid (pH 2.6) and acetonitrile were used as the mobile phase. The gradient elution program was 0–20% acetonitrile (10 min) followed by increasing to 35% (10 min), 60% (15 min) and 80% (10 min).

The concentration of H_2O_2 was determined by DPD method (Bader *et al.* 1988). The concentration of Fe was detected using an atomic absorption spectrophotometer (Varian, USA).

Electron spin resonance (ESR) analysis was performed on a Bruker model EPR 300E spectrometer (Bruker, Germany) equipped with a Quanta-Ray Nd:YAG laser (355 and 532 nm) to measure oxygen radicals spin-trapped by DMPO. Measurement conditions were center field 3,486.7 G, sweep width 100 G, microwave frequency 9.82 GHz, and power 5.05 mW.

RESULTS AND DISCUSSION

Characterization

UV-Vis analysis

From the UV-Vis spectra (Figure S4, Supplementary Information), pure TPyP in aqueous solution had a strong Soret-band at 420 nm and three relatively weak Q-bands at 517, 585 and 640 nm. The characteristic absorption at the Soret-band is mainly the transition of three electrons in the orbit of the porphyrin to the low energy orbit, and are assigned to the $\pi \rightarrow \pi^*$ ($a_{2u} \rightarrow e_R^*$) of the porphyrin ring. Three peaks at the Q-band are assigned to two relative N atoms among the four N atoms on the TPyP ring connected to H, which reduces molecular symmetry. Six hours after heating and reflux, characteristic peaks at the Soret-band widened and differentiated into two peaks (398 and 465 nm), and peaks at the Q-band reduced to only one peak at 525 nm, which indicated that the coordination between iron and central nitrogen of TPyP completed and FeTPyP was formed.

UV-Vis DRS analysis

The UV-Vis DRS spectra of FeTPyPY and NaY/Fe^{3+} are shown in Figure S5, indicating that UV-Vis absorption band wavelength shifted to the visible range when FeTPyP was supported on NaY. In the visible light region, NaY/Fe^{3+} had little absorption, while FeTPyPY had strong absorption, which demonstrated immobilized FeTPyPY facilitated absorption of visible light and broadened the response range (400–700 nm), evincing the visible catalytic performance.

IR spectrum of FeTPyPY

The IR spectrum of FeTPyPY is shown in Figure S6. The bands of 1,639 and 1,046 cm^{-1} were attributed to stretching vibration of C=N (pyridine). The band at 1,401 cm^{-1} indicated -OH existing in NaY. The bands at 792 and 716 cm^{-1} were assigned to bending vibration of C-H in the benzene ring and Ar-H, respectively. Two bands at 576 and 459 cm^{-1} were attributed to vibration of Fe-N, further demonstrating the coordination between iron and central nitrogen of TPyP.

Cyclic voltammetry of FeTPyPY

CV is an *in situ* technique to study the electrochemical properties of an electrode surface and its redox characteristics (Liu *et al.* 2013). Thus, it can be used to not only judge reversibility of electrode reaction, but also infer redox characteristics of the catalytic reaction, which is one of the most effective methods to explore the electrocatalytic mechanism. The CV of FeTPyPY was carried out in KOH solution (1 mol/L) at room temperature at potential from −0.05 to 0.05 V (versus SCE, Figure S7), which exhibited an oxidation peak at 0.403 V and reduction peak at 0.273 V, indicating immobilization catalyst FeTPyPY produced high redox peaks to improve the current efficiency and have good Fenton-like reaction characteristics.

TEM images

The surface characteristic of a catalyst directly affects its photocatalytic activity. Figure S8 shows TEM images of NaY/Fe^{3+} and FeTPyPY. Obviously, NaY-loaded Fe^{3+} had not dispersed successfully, which may be related to the

interaction of iron ions in NaY voids through ionic bonds or electrostatic interactions, while FeTPyPY was well dispersed, leading to better photocatalytic activity.

Photodegradation of MC-LR by FeTPyPY

Effect of pH

The degradation of MC-LR was carried out at different pH values. Results in Table 1 show that FeTPyPY has a high catalytic activity in a wide pH range (3.1–9.0), and the catalytic activity under neutral and acidic conditions is much better than that under alkaline condition. The Fenton-like catalyst FeTPyPY broadened the pH range. It was unlike the traditional (photo) Fenton system which was only effective in a medium of pH <3.0 (Zha *et al.* 2016). Furthermore, FeTPyPY was similar to the natural enzyme catalyzed reaction and had a higher activity under circumneutral pH condition (Song *et al.* 2013).

Kinetics of MC-LR photocatalytic degradation

The degradation kinetics of MC-LR by FeTPyPY and the comparative experiment without FeTPyPY are shown in Figure 1(a), which was treated as a pseudo-first order for plotting $\ln(c_t/c_0)$ against reaction time (t), displaying a straight line (Figure 1(b)).

$$\ln\frac{c_t}{c_0} = kt \tag{1}$$

$$t_{1/2} = \frac{\ln 2}{k} \tag{2}$$

where c_t and c_0 are the concentrations of MC-LR at time t and zero, respectively; k is the rate constant; $t_{1/2}$ is the half-life of MC-LR.

In the reaction, the concentration of MC-LR at time t was obtained from Equation (1). When the log of c(MC-LR) is plotted as a function of t, k is given by the slope, and $t_{1/2}$ of MC-LR can be calculated by Equation (2). For the degradation system in the presence and absence of FeTPyPY, k values were 0.00608 and 0.00006 min^{-1}, and $t_{1/2}$ values were 114 and 11,552 min, respectively. Results indicated the presence of FeTPyPY remarkably reduced the half-life of MC-LR by 99%.

Effect of humic acid on the degradation of MC-LR

Humic acid (HA), the primary NOM in natural waters (Fang *et al.* 2018) and an important photosensitizer, can have a significant effect on the indirect photolysis of MC-LR (Caupos *et al.* 2011). It may act as an inner filter to competitively absorb light and photons, leading to inhibiting effect on MC-LR removal (Zhou *et al.* 2013). Thus, the fate of MC-LR is greatly affected by the background value of HA in natural water bodies.

In our research, the degradation potential of FeTPyPY toward MC-LR in the presence of HA was investigated. Different concentrations of HA were added and results are shown in Figure 2. After 300 min of visible irradiation, 8% of MC-LR photolysis occurred, whereas with relatively high concentration of HA (100 mg/L), photolysis of MC-LR was inhibited. Due to the photosensitization of HA, MC-LR photolysis under solar irradiation was slightly enhanced at low HA concentration (<6.0 mg/L). However, further increase in HA concentration inhibited photolysis because of significant light competition or reactive oxygen species (ROS) quenching by HA (Niu *et al.* 2013). In the existence of FeTPyPY, MC-LR was successfully degraded even if the concentration of HA exceeded that of MC-LR by a factor of 10, 20 and 50. The results indicated that the photocatalytic degradation of MC-LR was not inhibited, but increased, which was significantly different to the previously reported phenomenon that the existence of HA clearly retarded MC-LR degradation due to ROS quenching (Li & Hu 2016). It strongly proved that MC-LR degradation by the prepared FeTPyPY was not affected by NOM.

Catalyst recycling

The recycling performance is significantly important for application in environmental technology (Wang *et al.* 2013). The reuse of FeTPyPY was evaluated for the degradation of MC-LR over seven cycles. After each cycle, the collected

Table 1 | Effect of pH on the degradation of MC-LR

	pH				
	3.1	5.3	7.0	9.0	11.2
Removal rate of MC-LR /%	62.5 ± 0.5	83.4 ± 0.8	92.7 ± 1.4	42.9 ± 0.3	15.2 ± 0.4

c(MC-LR) = 2 mg/L; c(FeTPyPY) = 1 g/L; reaction time = 300 min. Values of removal rates are mean ± standard deviations (n = 3).

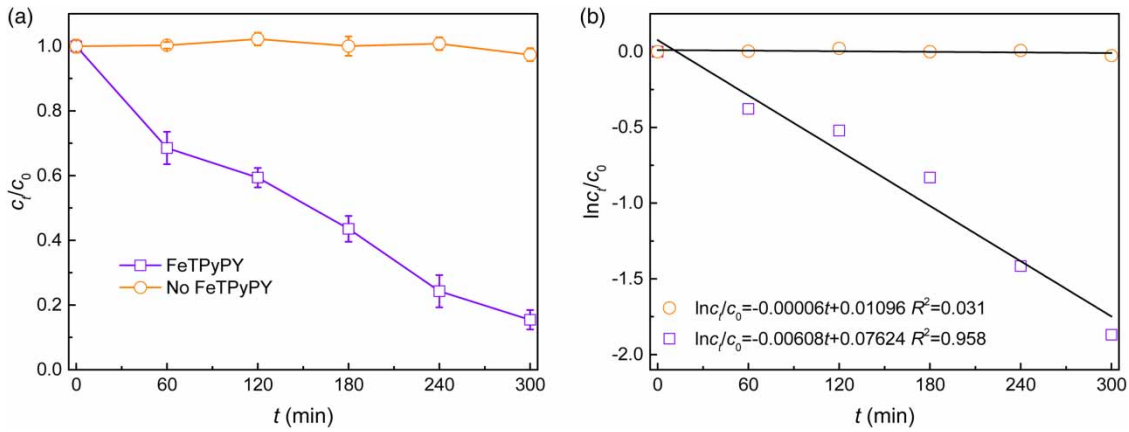

Figure 1 | Degradation of MC-LR by FeTPyPY (a) and reaction kinetics assuming pseudo-first order kinetics (b). c(MC-LR) = 2 mg/L; pH = 7.0; c(FeTPyPY) = 1 g/L. Error bars represent standard deviations of triplicate measurements (n = 3).

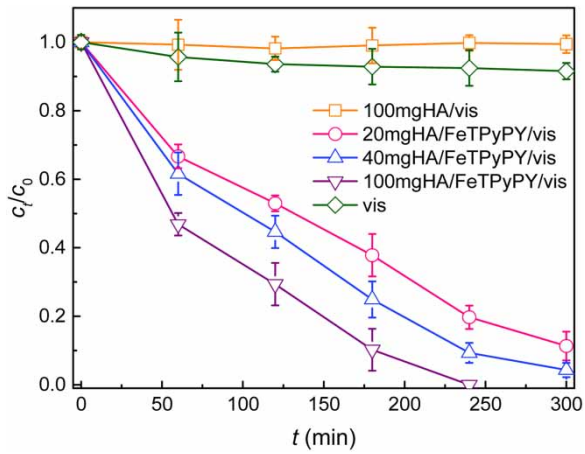

Figure 2 | The impact of HA on the degradation of MC-LR by FeTPyPY. c(MC-LR) = 2 mg/L; pH = 7.0; c(FeTPyPY) = 1 g/L. Error bars represent standard deviations of triplicate measurements (n = 3).

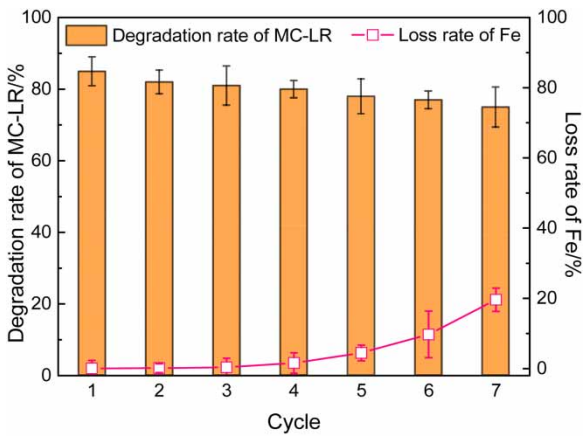

Figure 3 | Seven consecutive cycles of photodegradation with FeTPyPY and loss ratio of Fe during the process. c(MC-LR) = 2 mg/L; c(FeTPyPY) = 1 g/L; pH = 7.0. Error bars represent standard deviations of triplicate measurements (n = 3).

solution was filtered to obtain solid FeTPyPY, which was rinsed, dried and reused with identical experimental conditions. The results shown in Figure 3 demonstrated that the photocatalytic activity of FeTPyPY was maintained. Over seven consecutive cycles, FeTPyPY showed wonderful stability without attenuation. In addition, the loss of Fe in the solution was only 9.7% in continuous degradation of six cycles and reached 19.6% after seven cycles, leading to slight decrease of MC-LR degradation rate. At the end of the seventh cycle, the solution probably contained free iron ions and was used to degrade MC-LR under similar conditions, but no obvious degradation of MC-LR occurred, indicating the trace free iron ion existing in the solution was inactive. Moreover, the pH of the solution remained at approximately 7.0 during the cycle experiment. Furthermore, during the photoreaction process, no FeTPyP was found in

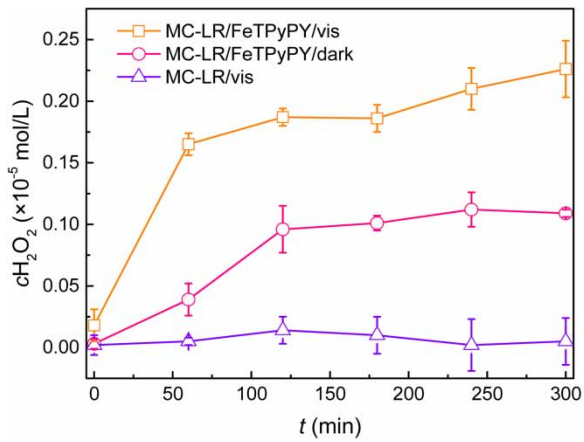

Figure 4 | Concentration changes of H_2O_2. c(MC-LR) = 2 mg/L; c(FeTPyPY) = 1 g/L; pH = 7.0. Error bars represent standard deviations of triplicate measurements (n = 3).

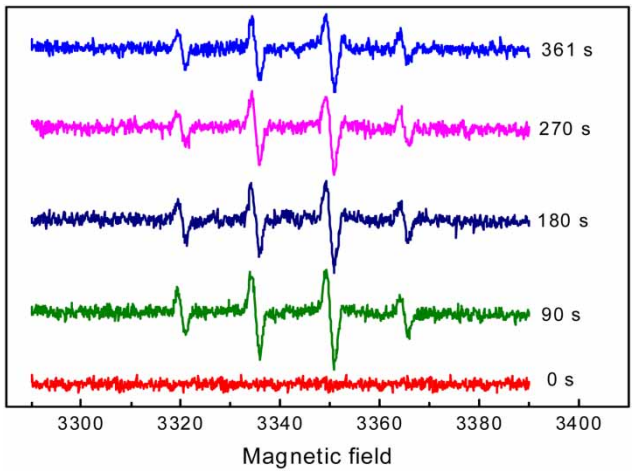

Figure 5 | ESR signals of the DMPO-•OH adducts in water. c(DMPO) = 0.04 mol/L; c(FeTPyPY) = 0.20 g/L.

the bulk solution. Results demonstrated that FeTPyPY was efficient and rather stable for the degradation of MC-LR in water under visible light irradiation.

Determination of H_2O_2 and •OH

The concentration of H_2O_2 was determined during the photocatalytic degradation process and the results are displayed in Figure 4. In the existence of FeTPyPY under visible light, the concentration of H_2O_2 increased with illumination time, indicating H_2O_2 was an intermediate oxidant. It was noted that H_2O_2 was stable under acid condition while easy to be decomposed under alkaline condition, leading to bad performance of FeTPyPY under alkaline condition (Table 1). Control experiments that tracked H_2O_2 change with time were also run with FeTPyPY in the dark. Without FeTPyPY or visible light, the concentration of H_2O_2 was negligible, consistent with the results of slow degradation of MC-LR under similar conditions.

The •OH formation was measured qualitatively by ESR, which is an up-to-date analytical technique used to determine short-lived free radicals and is useful for elucidating photocatalytic reaction mechanisms (Li *et al.* 2016). As shown in Figure 5, no obvious ESR signals were observed in

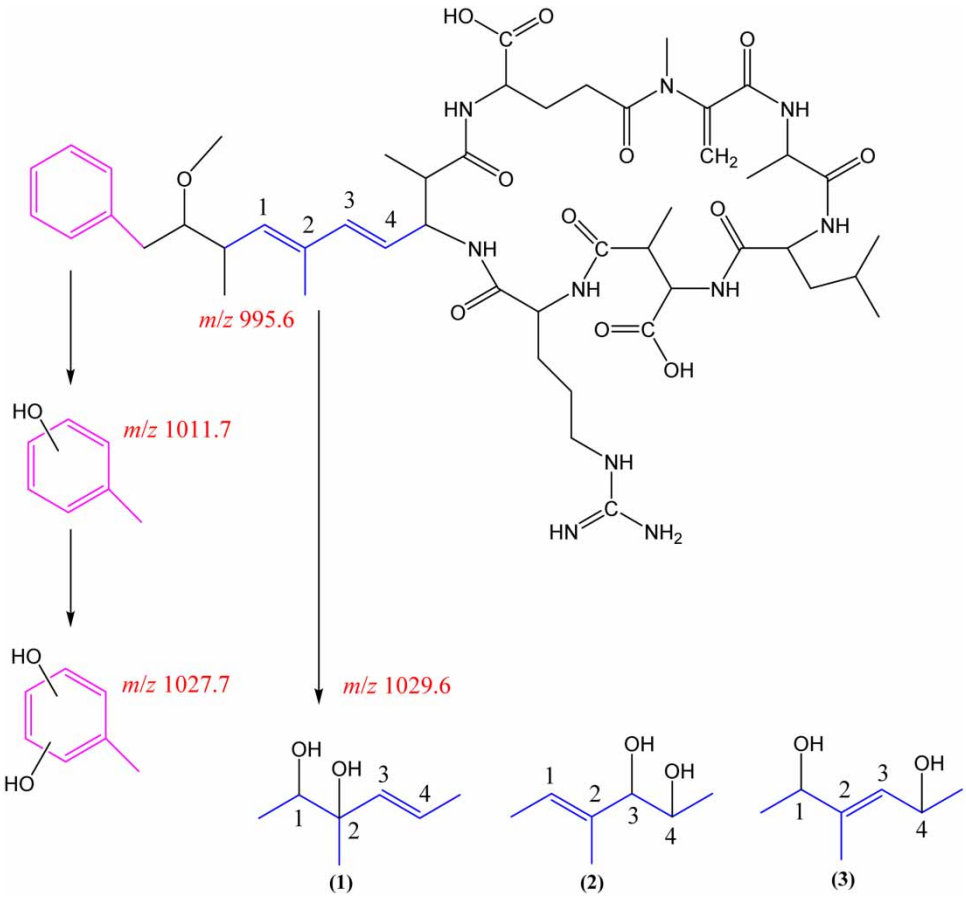

Figure 6 | Hydroxylation products of the conjugated double bonds on the Adda chain and the aromatic ring of MC-LR.

the reaction without visible light, whereas under visible light irradiation, characteristic quartet peaks of DMPO-˙OH adduct appeared with an intensity ratio of 1:2:2:1 and stabilized after 90 s of irradiation. The result indicated that the degradation of MC-LR by FeTPyPY involved ˙OH, which is an intermediate species in photocatalytic reactions.

Possible degradation pathway

In order to reveal the degradation pathway, reaction intermediates of MC-LR degradation by FeTPyPY under visible light irradiation were analyzed utilizing LC/MS. Total ion chromatogram results (Figure S9) showed that initial degradation products were primarily hydroxylated products *m/z* 1,029.6, *m/z* 1,011.7 and *m/z* 1,027.7 (Figure 6). There were three isomers of *m/z* 1,029.6, two 1,2-addition products (1 and 2) and a 1,4-addition product (3), corresponding to hydroxyl addition of the conjugated double bonds on the Adda of MC-LR. Due to relative instability of products 1 and 2, *m/z* 1,029.5 (1) was further oxidized to ketone compound *m/z* 835.4 and aldehyde compound *m/z* 795.3, while *m/z* 1,029.5 (1) was directly oxidized to

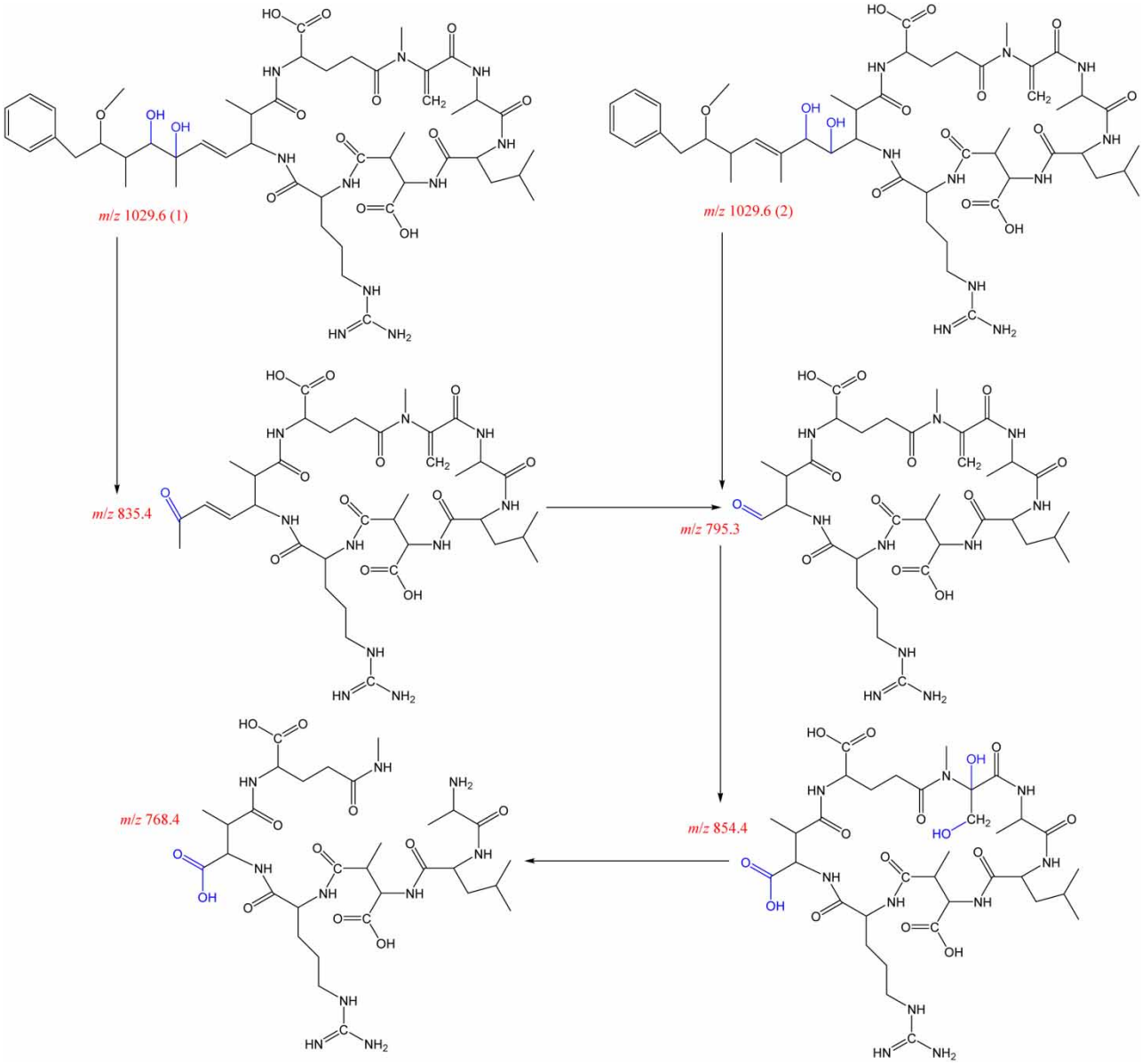

Figure 7 | Degradation pathway of *m/z* 1,029.6.

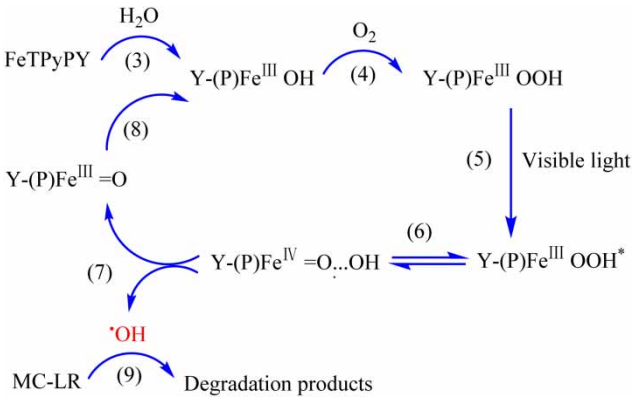

Figure 8 | Proposed mechanism for the degradation of MC-LR illuminated by visible light.

aldehyde compound *m/z* 795.3. Hydroxyl radical attacked the unsaturated C=C at *m/z* 795.3, and product *m/z* 854.4 was generated. With triplicate oxidative decarboxylation, bond cleavage happened at product *m/z* 854.4 and product *m/z* 768.4 was generated at last (Figure 7).

Proposed photodegradation mechanism

A remarkable feature is the enhanced photocatalytic efficiency of FeTPy after immobilizing onto NaY. The catalytic activity of FeTPy in this heterogeneous system is remarkably enhanced compared to that in a homogeneous system (Figure 1(a)). On the basis of all experimental results, a possible mechanism for the photocatalytic system is proposed, represented schematically in Figure 8, to explain the activity enhancement of the immobilized FeTPyPY. On the surface of hydrophobic FeTPyPY, H_2O easily approaches the iron center of FeTPyPY at the axial direction to give axial ligand Y-(P)Fe^{III}OH (Equation (3) in Figure 8), which may contact with dissolved oxygen in water to form a new ligand Y-(P)Fe^{III}OOH at another axial direction (Equation (4)). Under visible light irradiation, Y-(P)Fe^{III}OOH is activated to produce excited state Y-(P)Fe^{III}OOH* (Equation (5)). Electron transfer between iron and ligand of FeTPyPY occurs and transient species Y-(P)Fe^{IV}=O…OH (Equation (6)) forms. However, Y-(P)Fe^{IV}=O…OH is unstable, resulting in the O-O band of Y-(P)Fe^{IV}=O…OH easily undergoing rapid cleavage to generate •OH and Y-(P)Fe^{III}=O (Equation (7)). Y-(P)Fe^{III}=O can convert to Y-(P)Fe^{III}OH (Equation (8)). A redox cycle is completed and the net result is generation of •OH, a highly active species that can degrade MC-LR effectively (Equation (9)). In all, the degradation of MC-LR relied on •OH generated during the redox cycle. Therefore, FeTPyPY would be useful for degradation of other congeners which usually co-occur in surface water.

CONCLUSIONS

Highly toxic MC-LR has been shown to undergo photodecomposition in aqueous solution under visible light, using a photocatalytic oxidation system consisting of FeTPyP immobilized on NaY, by tracking oxygen species in the oxidation process. Under visible irradiation, 85% of MC-LR was efficiently degraded by immobilized FeTPyPY after 300 min of visible light illumination. The immobilized photocatalyst FeTPyPY can be easily collected from the reaction solution by simple filtration and reused for photocatalysis with scarce loss of activity. This photocatalytic system provides an additional approach, with great potential, for the oxidative removal of persistent organic pollutants. In industrial water treatment, immobilized FeTPyPY is expected to be used in fixed bed reactors to continuously degrade toxins besides MC-LR. Compared with other methods, it would be cost-efficient as no other oxidant is needed and it has high sustained activity.

FUNDING

This work was supported by the National Natural Science Foundation of China (Nos. 51909082, 51808202, 31800457) and the Natural Science Foundation of Hubei Province (No. 2016CFB190). Authors thank the anonymous reviewers for their comments.

CONFLICTS OF INTEREST

The authors declare no conflict of interest.

SUPPLEMENTARY MATERIAL

The Supplementary Material for this paper is available online at https://dx.doi.org/10.2166/wst.2020.083.

REFERENCES

Aschermann, G., Jeihanipour, A., Shen, J., Mkongo, G., Dramas, L., Croue, J. P. & Schäfer, A. 2016 Seasonal variation of organic matter concentration and characteristics in the Maji ya Chai River (Tanzania): impact on treatability by ultrafiltration. *Water Research* **101**, 370–381.

Bader, H., Sturzenegger, V. & Hoigné, J. 1988 Photometric method for the determination of low concentrations of hydrogen

peroxide by the peroxidase catalyzed oxidation of N, N-diethyl-*p*-phenylenediamine (DPD). *Water Research* **22** (9), 1109–1115.

Brunberg, A. K. & Blomqvist, P. 2002 Benthic overwintering of *Microcystis* colonies under different environmental conditions. *Journal of Plankton Research* **24** (11), 1247–1252.

Caupos, E., Mazellier, P. & Croue, J. P. 2011 Photodegradation of estrone enhanced by dissolved organic matter under simulated sunlight. *Water Research* **45** (11), 3341–3350.

Fang, Y., Zhou, W., Tang, C., Huang, Y., Johnson, D. M., Ren, Z. J. & Ma, W. 2018 Brönsted catalyzed hydrolysis of microcystin-LR by siderite. *Environmental Science & Technology* **52** (11), 6426–6437.

Gamelas, S. R. D., Gomes, A. T. P. C., Moura, N. M. M., Faustino, M. A. F., Cavaleiro, J. A. S., Lodeiro, C., Veríssimo, M. I. S., Fernandes, T., Daniel-da-Silva, A., Gomes, M. T. S. R. & Neves, M. G. P. M. S. 2018 *N*-Confused porphyrin immobilized on solid supports: synthesis and metal ions sensing efficacy. *Molecules* **23** (4), 867–882.

Günay, T. & Cimen, Y. 2017 Degradation of 2,4,6-trichlorophenol with peroxymonosulfate catalyzed by soluble and supported iron porphyrins. *Environmental Pollution* **231** (2017), 1013–1020.

Han, J., Jeon, B., Futatsugi, N. & Park, H. D. 2013 The effect of alum coagulation for in-lake treatment of toxic *Microcystis* and other cyanobacteria related organisms in microcosm experiments. *Ecotoxicology and Environmental Safety* **96**, 17–23.

Henao, E., Rzymski, P. & Waters, M. N. 2020 A review on the study of cyanotoxins in paleolimnological research: current knowledge and future needs. *Toxins* **12** (1), 2–15.

Holst, T., Jørgensen, N. O. G., Jørgensen, C. & Johansen, A. 2003 Degradation of microcystin in sediments at oxic and anoxic, denitrifying conditions. *Water Research* **37**, 4748–4760.

Hu, C. & Rzymski, P. 2019 Programmed cell death-like and accompanying release of microcystin in freshwater bloom-forming cyanobacterium microcystis: from identification to ecological relevance. *Toxins* **11** (706), 2–19.

Katz, J. E., Zhang, X., Attenkofer, K., Chapman, K. W., Frandsen, C., Zarzycki, P., Rosso, K. M., Falcone, R. W., Waychunas, G. A. & Gilbert, B. 2012 Electron small polarons and their mobility in iron (oxyhydr)oxide nanoparticles. *Science* **337** (6099), 1200–1203.

Kim, J. H., Kwon, H., Lee, S. & Lee, C. H. 2005 Removal of endocrine disruptors using homogeneous metal catalyst combined with nanofiltration membrane. *Water Science and Technology* **51** (6–7), 381–390.

Krzywicka, A. & Kwarciak-Kozłowska, A. 2014 Advanced oxidation processes with coke plant wastewater treatment. *Water Science and Technology* **69** (9), 1875–1878.

Li, S. & Hu, J. 2016 Photolytic and photocatalytic degradation of tetracycline: effect of humic acid on degradation kinetics and mechanisms. *Journal of Hazardous Materials* **318**, 134–144.

Li, Y., Xiao, J., Shubina, T. E., Chen, M., Shi, Z., Schmid, M., Steinrück, H.-P., Gottfried, J. M. & Lin, N. 2012 Coordination and metalation bifunctionality of Cu with 5,10,15,20-tetra (4-pyridyl) porphyrin: toward a mixed-valence two-dimensional coordination network. *Journal of the American Chemistry Society* **134** (14), 6401–6408.

Li, J., Lin, H., Yang, L. & Zhang, H. 2016 Copper-spent activated carbon as a heterogeneous peroxydisulfate catalyst for the degradation of Acid Orange 7 in an electrochemical reactor. *Water Science and Technology* **73** (8), 1802–1808.

Li, W., Xu, X., Lyu, B., Tang, Y., Zhang, Y., Chen, F. & Korshin, G. 2019 Degradation of typical macrolide antibiotic roxithromycin by hydroxyl radical: kinetics, products, and toxicity assessment. *Environmental Science and Pollution Research* **26** (14), 14570–14582.

Liu, S., Zhao, X., Sun, H., Li, R., Fang, Y. & Huang, Y. 2013 The degradation of tetracycline in a photo-electro-Fenton system. *Chemical Engineering Journal* **231**, 441–448.

Mantzouki, E., Lürling, M., Fastner, J., Domis, L. S., Wilk-Wozniak, E., Koreiviene, J., Seelen, L., Teurlincx, S., Verstijnen, Y., Krzton, W., Walusiak, E., Karosiene, J., Kasperoviciene, J., Savadova, K., Vitonyte, I., Cillero-Castro, C., Budzynska, A., Goldyn, R., Kozak, A., Rosinska, J., Szelag-Wasielewska, E., Domek, P., Jakubowska-Krepska, N., Kwasizur, K., Messyasz, B., Pełechata, A., Pełechaty, M., Kokocinski, M., García-Murcia, A., Real, M., Romans, E., Noguero-Ribes, J., Duque, D. P., Fernández-Morán, E., Karakaya, N., Häggqvist, K., Demir, N., Beklioglu, M., Filiz, N., Levi, E., Iskin, U., Bezirci, G., Tavsanoglu, Ü. N., Özhan, K., Gkelis, S., Panou, M., Fakioglu, Ö., Avagianos, C., Kaloudis, T., Çelik, K., Yilmaz, M., Marcé, R., Catalán, N., Bravo, A. G., Buck, M., Colom-Montero, W., Mustonen, K., Pierson, D., Yang, Y., Raposeiro, P. M., Gonçalves, V., Antoniou, M. G., Tsiarta, N., McCarthy, V., Perello, V. C., Feldmann, T., Laas, A., Panksep, K., Tuvikene, L., Gagala, I., Mankiewicz-Boczek, J., Yagci, M. A., Çinar, S., Çapkin, K., Yagci, A., Cesur, M., Bilgin, F., Bulut, C., Uysal, R., Obertegger, U., Boscaini, A., Flaim, G., Salmaso, N., Cerasino, L., Richardson, J., Visser, P. M., Verspagen, J. M. H., Karan, T., Soylu, E. N., Maraslioglu, F., Napiórkowska-Krzebietke, A., Ochocka, A., Pasztaleniec, A., Antão-Geraldes, A. M., Vasconcelos, V., Morais, J., Vale, M., Köker, L., Akçaalan, R., Albay, M., Maronic, D. Š., Stevic, F., Pfeiffer, T. Ž., Fonvielle, J., Straile, D., Rothhaupt, K., Hansson, L., Urrutia-Cordero, P., Bláha, L., Geriš, R., Fránková, M., Koçer, M. A. T., Alp, M. T., Remec-Rekar, S., Elersek, T., Triantis, T., Zervou, S. K., Hiskia, A., Haande, S., Skjelbred, B., Madrecka, B., Nemova, H., Drastichova, I., Chomova, L., Edwards, C., Sevindik, T. O., Tunca, H., Önem, B., Aleksovski, B., Krstic, S., Vucelic, I. B., Nawrocka, L., Salmi, P., Machado-Vieira, D., Oliveira, A. G., Delgado-Martín, J., García, D., Cereijo, J. L., Gomà, J., Trapote, M. C., Vegas-Vilarrúbia, T., Obrador, B., Grabowska, M., Karpowicz, M., Chmura, D., Úbeda, B., Gálvez, J. Á., Özen, A., Christoffersen, K. S., PerltWarming, T., Kobos, J., Mazur-Marzec, H., Pérez-Martínez, C., Ramos-Rodríguez, E., Arvola, L., Alcaraz-Párraga, P., Toporowska, M., Pawlik-Skowronska, B., Niedzwiecki, M., Peczuła, W., Leira, M., Hernández, A., Moreno-Ostos, E., Blanco, J. M., Rodríguez, V., Montes-Pérez, J. J., Palomino, R. L., Rodríguez-Pérez, E., Carballeira, R., Camacho, A., Picazo, A., Rochera, C.,

Santamans, A. C., Ferriol, C., Romo, S., Soria, J. M., Dunalska, J., Sienska, J., Szymanski, D., Kruk, M., Kostrzewska-Szlakowska, I., Jasser, I., Žutinic, P., Udovic, M. G., Plenković-Moraj, A., Frak, M., Bankowska-Sobczak, A., Wasilewicz, M., Özkan, K., Maliaka, V., Kangro, K., Grossart, H. P., Paerl, H. W., Carey, C. C. & Ibelings, B. W. 2018 Temperature effects explain continental scale distribution of cyanobacterial toxins. *Toxins* **10** (156), 1–24.

Niu, J., Li, Y. & Wang, W. 2013 Light-source-dependent role of nitrate and humic acid in tetracycline photolysis: kinetics and mechanism. *Chemosphere* **92** (11), 1423–1429.

Peng, G., Fan, Z., Wang, X., Sui, X. & Chen, C. 2015 Photodegradation of microcystin-LR catalyzed by metal phthalocyanines immobilized on TiO_2-SiO_2 under visible-light irradiation. *Water Science and Technology* **72** (10), 1824–1831.

Phujomjai, Y., Somdee, A. & Somdee, T. 2015 Biodegradation of microcystin [Dha^7]MC-LR by a novel microcystin-degrading bacterium in an internal airlift loop bioreactor. *Water Science and Technology* **73** (2), 267–274.

Rahimi, R., Shokraiyan, J., Rabbani, M. & Fayyaz, F. 2015 Enhanced photobactericidal activity of ZnO nanorods modified by meso-tetrakis(4-sulfonatophenyl)porphyrin under visible LED lamp irradiation. *Water Science and Technology* **71** (8), 1249–1254.

Schreiner, E., Nair, N. N., Wittekindt, C. & Marx, D. 2011 Peptide synthesis in aqueous environments: the role of extreme conditions and pyrite mineral surfaces on formation and hydrolysis of peptides. *Journal of the American Chemical Society* **133** (21), 8216–8226.

Song, W. J., Sun, Y. J., Choi, S. K. & Nam, W. 2005 Mechanistic insights into the reversible formation of iodosylarene-iron porphyrin complexes in the reactions of oxoiron (IV) porphyrin π-cation radicals and iodoarenes: equilibrium, epoxidizing intermediate, and oxygen exchange. *Chemistry: A European Journal* **12** (1), 130–137.

Song, Q., Jia, M., Ma, W., Fang, Y. & Huang, Y. 2013 Heterogeneous degradation of toxic organic pollutants by hydrophobic copper Schiff-base complex under visible irradiation. *Science China Chemistry* **56**, 1775–1782.

Sorokin, A., Suzzoni-Dezard, S. D., Poullain, D., Noël, J.-P. & Meunier, B. 1996 CO_2 as the ultimate degradation product in the H_2O_2 oxidation of 2,4,6-trichloropenol catalyzed by iron tetrasulfophthalocyanine. *Journal of the American Chemistry Society* **118** (31), 7410–7411.

Tang, Y., Liu, H., Zhou, L., Ren, H., Li, H., Zhang, J., Chen, G. & Qu, C. 2019 Enhanced Fenton-like oxidation of hydroxypropyl guar gum catalyzed by EDTA-metal complexes in a wide pH range. *Water Science and Technology* **79** (9), 1667–1674.

Wang, S., Ma, W., Jia, M. & Huang, Y. 2013 Degradation of pollutants by hydrophobic $FePcCl_{16}$ under ultraviolet and visible light. *Fresenius Environmental Bulletin* **22** (2), 549–555.

Wang, L., Jin, P., Duan, S., Huang, J., She, H., Wang, Q. & An, T. 2019 Accelerated Fenton-like kinetics by visible-light-driven catalysis over iron(III) porphyrin functionalized zirconium MOF: effective promotion on the degradation of organic contaminants. *Environmental Science: Nano* **6**, 2652–2661.

Yanina, S. V. & Rosso, K. M. 2008 Linked reactivity at mineral-water interfaces through bulk crystal conduction. *Science* **320**, 218–222.

Yasmin, R., Aftab, K. & Kashif, M. 2019 Removal of microcystin-LR from aqueous solution using *Moringa oleifera* Lam. seeds. *Water Science and Technology* **79** (1), 104–113.

Zha, Y., Zhou, Z., He, H., Wang, T. & Luo, L. 2016 Nanoscale zero-valent iron incorporated with nanomagnetic diatomite for catalytic degradation of methylene blue in heterogeneous Fenton system. *Water Science and Technology* **73** (11), 2815–2823.

Zhou, L., Ji, Y. F., Zeng, C., Zhang, Y., Wang, Z. & Yang, X. 2013 Aquatic photodegradation of sunscreen agent *p*-aminobenzoic acid in the presence of dissolved organic matter. *Water Research* **47** (1), 153–162.

First received 22 August 2019; accepted in revised form 17 February 2020. Available online 25 February 2020